In Vitro Magnetic Resonance Assessment of Tissue Engineered Bone and Cartilage

BY

HEMANTI CHAVADA

B.Tech, Gujarat Technological University, India, 2013

THESIS

Submitted as partial fulfillment of the requirements

for the degree of Master of Science in Bioengineering

in the Graduate College of the

University of Illinois at Chicago, 2016

Chicago, Illinois

Defense committee:

      Dr. Richard L. Magin, Chair and Advisor

      Dr. Mrignayani Kotecha, Advisor

      Dr. Dieter Klatt

      Dr. Sriram Ravindran, Department of Oral Biology

This thesis is dedicated to my loving parents and my brother for their belief in me and their continuous support.

ACKNOWLEDGEMENTS

Firstly, I would like to thank my thesis advisor Dr. Magin for being instrumental in introducing me to the field of MRI. He not only provided me guidance but have encouraged me during difficult times and always motivated to work harder. I would also like to extend my deepest gratitude to Dr. Mrignayani Kotecha who played a pivotal role in my research and without her guidance and insights this research wouldn't have been possible.

I would like to thank Dr. Sriram Ravindran and Dr.Chun-Chieh Huang for their contribution that have helped in accomplishment of this research. I would like to thank Dr. Rob Kleps who taught me my first MRI scan and Dr. Weiguo Li for his efforts and providing his invaluable assistance whenever I needed. A special thanks to my lab mates Shreyan Majumdar and Vidyani Suryadevara for training, assistance and suggestions that contributed to this study.

Finally, I express my profound gratitude to my family and my friends for providing me with unfailing support and continuous encouragement. This accomplishment would not have been possible without their love and support.

TABLE OF CONTENTS

Chapter   Page

LIST OF TABLES

LIST OF FIGURES

LIST OF ABBREVIATIONS

ADC	Apparent Diffusion Coefficient
CPMG	Car Purcell Meiboom Gill
DTI	Diffusion Weighted Imaging
ECM	Extracellular Matrix
FID	Free Induction Decay
FOV	Field of View
FT	Fourier Transform
HMSCs	Human marrow stromal cells
LZ	Leucine Zipper
MR	Magnetic Resonance
MRI	Magnetic Resonance Imaging
MSME	Multi Slice Multi Echo
NMR	Nuclear Magnetic Resonance
RARE	Rapid Acquisition with Refocused Echoes
RAREVTR	RARE with variable Repetition Time
RF	Radio Frequency
TE	Echo Time
TERM	Tissue Engineering Regenerative Medicine
TR	Repetition Time

SUMMARY

Magnetic Resonance Imaging (MRI), largely due to its noninvasive nature, is a powerful tool for the characterization of early structural and compositional changes in engineered tissues. For example, the development of extracellular matrix (ECM) is reflected in decreasing values of the MR derived relaxation times and diffusion coefficients. Hence, the regeneration and repair of any tissue, which requires a scaffold, appropriate cell types, and growth factors, can be monitored using MRI. This study identified early structural changes in two types of engineered tissues: engineered cartilage and engineered bone. The MRI measurements were performed using the Bruker 500 MHz (11.7 T) microimaging facility located in the Research Resources Center at UIC.

The tissue-engineered cartilage constructs were prepared by seeding human marrow stromal cells (HMSCs) in commercially available collagen scaffolds under two different set of conditions: (a) hypoxia – constructs created under low oxygen conditions, and (b) normoxia – constructs created under normal oxygen conditions.

Tissue engineered bone constructs were prepared using Leucine Zipper (LZ) based biomimetic scaffolds with low and high levels of osteogenic extracellular matrix (ECM). The T_1 and T_2 relaxation times fell as we move from low to high ECM in engineered bone and from normal to hypoxic conditions in engineered cartilage; both changes are consistent with higher amount of ECM generated in these constructs.

Measurements of the average diffusion coefficient for these tissues was not statistically significant between the groups. These results show that MRI relaxation times are sensitive to small growth changes in tissue engineered cartilage and bone and hence could be used as biomarkers for tissue regeneration.

1. INTRODUCTION

1.1 Background

Over the years Magnetic Resonance Imaging (MRI) has emerged as a powerful method to image the internal organs and structures of our body and it gives the spatial information that cannot be obtained through other imaging modalities. MRI is known as the safest way among the imaging modalities due to its noninvasive nature of acquiring information form the problem areas for example: tumors, injury, bleeding, infection or diseases in the blood vessels etc. The images obtained through the MRI scans are of high resolution that makes MRI the best technique to see abnormal changes in the body.

1.2 Motivation

One of the most advanced regenerative techniques in tissue engineering regenerative medicine (TERM) is connective tissue engineering such as bone and cartilage tissue engineering, which has been developed to replace damaged bone and cartilage with a newly grown tissue to establish a complete repair and regeneration. It is not yet achieved to completely repair and regenerate native like cartilage thus improvements in these techniques are currently being investigated. At all levels of tissue engineering the need of assessment is necessary. Therefore, a noninvasive technique is required to monitor the structural and compositional changes of tissue engineered chondrogenic and osteogenic scaffolds. MRI is a technique sensitive in detecting changes in tissue structure noninvasively and is great in evaluating the mechanical and biochemical changes without

destructing the tissue engineered bone and cartilage scaffolds in vitro or sacrificing the animal model used for in vivo experiments.

In the first study, osteogenic constructs made out of Leucine Zipper based hydrogels (LZ) were used. Leucine Zipper based self-assembling hydrogels have advantage over traditional hydrogels as they provide more robust control over hydrogel. Synthesis of extracellular matrix integrated LZ hydrogels with tunable properties does not require delivery of growth factors, therefore creating new opportunities for regenerative tissue engineering (3). In the first study, we characterize LZ based scaffolds by establishing MRI characterization protocols. We take two sets of LZ based scaffolds: low and high ECM integrated and perform MRI measurements to determine the structural and mechanical properties of the tissue.

In the second study, MRI measurements were performed on commercially available Zimmer Clinical grade collagen tape modified under two sets of conditions: normoxic (normal) and hypoxic (low) oxygen conditions to improve their properties for clinical use. MRI studies were performed to study the properties of modified scaffolds in order to determine their structural and mechanical properties boosted for better performance in clinical use.

2. THEORY

2.1 Magnetic Resonance Imaging

The beauty of biomedical imaging modalities lies in their noninvasive nature and MRI being completely noninvasive (devoid of ionizing radiation exposure) has emerged as the most powerful tool among other imaging techniques. MRI derived its concept from Nuclear Magnetic Resonance (NMR) and the concept of magnetic resonance was discovered by two physicists, Felix Bloch and Edward Mills Purcell. NMR spectroscopy was used to study the composition of chemical compounds, but it was Paul Lauterbur and Peter Mansfield who accomplished producing 2D images with use of NMR (10). They were awarded Nobel Prize in 2003 for their discoveries related to Magnetic Resonance Imaging.

2.1.1 MRI Fundamentals

Protons are the main signal source of MRI because they behave like tiny magnets and they are available in abundance in body (fat and water). Proton, a positively charged particle found in atomic nuclei, is constantly spinning about its axis resulting in a magnetic moment μ. The magnetic moment of proton can be considered as a vector with a direction and finite size and is directly proportional to the angular momentum I,

$$\mu = \gamma I \qquad (2.1)$$

where γ is gyromagnetic ratio (characteristic of nuclei).

The net magnetization (M_0) is the vector sum of these magnetic moments. In the absence of magnetic field, protons are randomly oriented cancelling out each other, thus the net magnetization becomes zero. When an external magnetic field B_0 is applied, protons are arranged either parallel (low energy state) or anti-parallel to the field (high energy state). There are more protons aligned parallel to the magnetic field causing net magnetization in the direction of the magnetic field (10, 13).
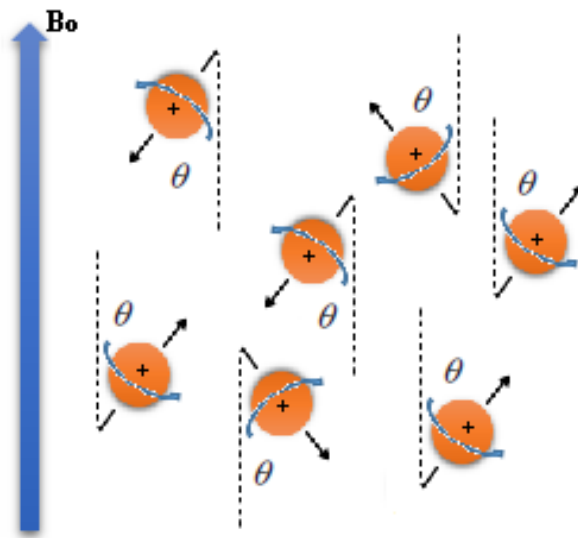
Figure 1: Schematic diagram of Protons aligned parallel and anti-parallel to B_0 (adapted from 10)

The external magnetic field causes protons to precess at an angle θ about the magnetic field. The combined effect of the force from the external magnetic field and the spinning motion causes the protons to precess. It is important to know the precessional frequency of the proton in order to determine the operating frequency of the MRI system.

This precessional frequency is proportional to the strength of the external magnetic field and can be determined by Larmor equation:

$$\omega_0 = \gamma B_0 \qquad\qquad (2.2)$$
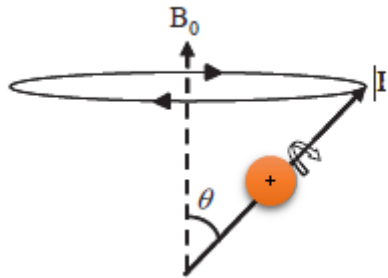
Figure 2: A schematic diagram of proton spin precessing about B_0 with an angular momentum I (adapted from10).

The gyromagnetic ratio (MHz/T) of few imaged isotopes are listed in the table below:

H-1	42.58
F-19	40.05
Na-23	11.26
P-31	17.24

Table 1: Gyromagnetic ratio of few isotopes that can be used as MRI signal source (14).

Once the protons achieve equilibrium with the external magnetic field B_0, they continue to be aligned and precess about B_0. This equilibrium is disturbed when they are bombarded with radiofrequency energy (B_1) equivalent to their precessional frequency,

following which protons shift to high energy state. When the radiofrequency energy is turned off, the proton revert to its original low energy state giving off RF energy in the process. This energy is the MRI signal (14).
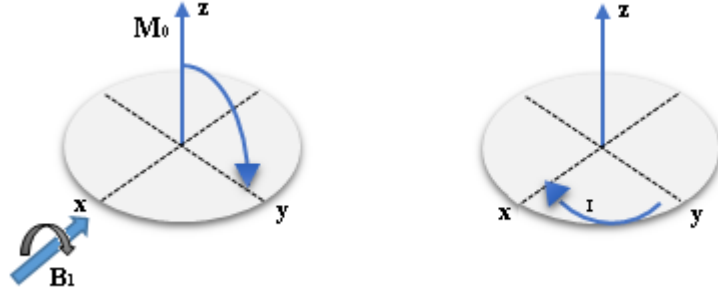
Figure 3: Flipping of net magnetization to transverse plane after the application of RF energy (adapted form 10, 13).

It is necessary to apply radiofrequency energy equivalent to Larmor frequency to match the difference in energy levels (ΔE) of proton spins under constant magnetic field B_0. This creates a condition known as resonance which leads to efficient transfer of energy from RF coil to the protons. Energy transfer can be calculated through De Broglie's relationship:

$$hf = \Delta E = \frac{hB_0\gamma}{2\pi} \tag{2.3}$$

$$f = \frac{hB_0\gamma}{2\pi} \text{ or } \omega_0 = \frac{hB_0\gamma}{2\pi} \tag{2.4}$$

2.1.2 Spin-lattice (T_1) Relaxation

When a 90 degree RF pulse is applied, the protons precessing about the magnetic field acquire energy and the net magnetization $M_0 = M_z$, flip to the transverse xy plane. After the pulse is switched off, the protons will start relaxing to original state i.e., aligning themselves to the vertical plane giving off excess energy acquired once the RF pulse is turned off with a time constant T_1. The T_1 curve is shown in figure 4. The T_1 relaxation is known as spin-lattice relaxation time. The rate at which M_z recovers to M_0 is characterized by:

$$M_z(t) = M_0(1 - e^{\frac{-t}{T_1}}) \qquad (2.5)$$

T_1 is defined as the time taken by longitudinal magnetization to reach 63% of its final value. The proton relaxation rates vary for different tissues and can range from hundreds to thousands of milliseconds (10, 13, 14).
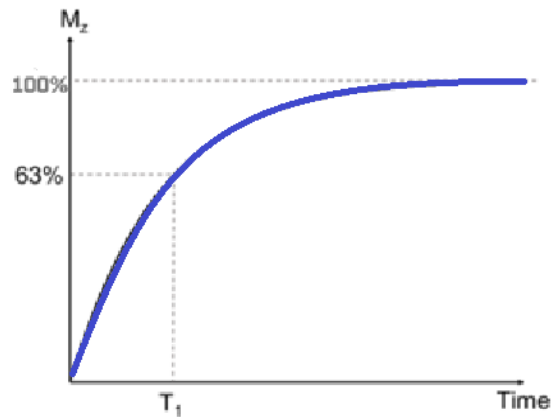
Figure 4: T_1 relaxation curve.

2.1.3 Spin-Spin relaxation (T$_2$) Decay

When the magnetization is flipped to the transverse plane the protons continues to precess around the vertical axis. At t=0, all the magnetic moments are in phase and we get maximum signal at that time. The transverse magnetization starts to decay due to interactions between spins while interacting with tissue. These interactions between the spins cause decay in the signal. The vector sum of the magnetic moments gradually decays to zero. The rate at which M$_{xy}$ decays can be characterized by

$$M_{xy} = M_0 \left(e^{\frac{-t}{T_2}} \right) \tag{2.6}$$

T$_2$ decay is also known as spin-spin relaxation time. Unlike T$_1$, there is no net loss of energy in T$_2$ decay and the relaxation time is in order of tens of milliseconds in most tissues. The value of T$_2$ is shorter for solids than liquids and the difference in the values T$_1$ and T$_2$ for different tissues becomes the source of MR contrast in MRI images (10).
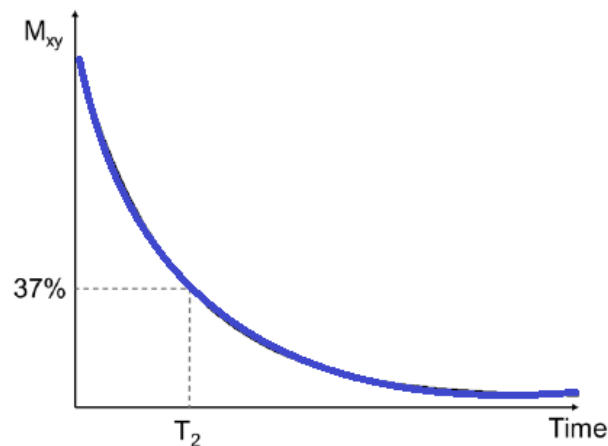
Figure 5: T$_2$ Dephasing.

2.1.4 <u>Free induction decay</u>

The primary transient signal in MRI is the free induction decay (FID) signal. The decaying transverse magnetization, M_{xy}, induces an electrical current in the RF coil whereas longitudinal magnetization will not. Once the RF pulse is turned off, transverse magnetization M_{xy} will precess about z-direction and this oscillating signal will decay as the function of time. This is known as free induction decay.
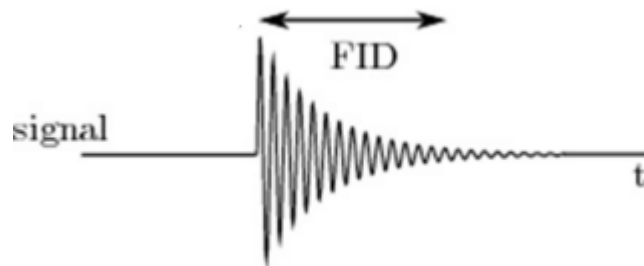
Figure 6: Free induction decay (FID).

2.1.5 <u>Encoding</u>

Any Imaging systems obtains the image in two steps: In the first step, the spatial information is encoded in a measurable signal and in second step the encoded signal is decoded to produce an image. In MRI, acquiring NMR signal accomplishes the spatial encoding process. Encoding comprises of two things: slice selection and spatial encoding within the slice (10, 13).

- Slice selection: A slice-selective RF excitation pulse is applied that excites the spins in the chosen particular slice.

- Spatial encoding within the slice: Application of frequency encoding and phase encoding gradients which allow the encoding of spatial location.

- The frequency encoding gradient: Encodes signals into different frequencies, depending upon the spatial information towards the gradient

- The phase encoding gradient encodes the spatial signal location by different spin phases. The number of phase encoding gradients is directly related to the spatial resolution.

- K-space: The space covered by the phase encoding and frequency encoding data. There are number of points in the k-space and they are dictated by the number of phase encoding steps and frequency encoding steps in the pulse sequence. The image is obtained once all the k-space has been assembled and Fourier transform is applied to it (10, 13, 14).

2.1.6 MRI Hardware

There are three major hardware components of MRI: a) Magnet (typically superconducting), b) Radiofrequency transmitter and receiver and c) A set of three gradient coils (X, Y, Z).

a) Magnet: The most important and expensive component of the MRI system is magnet. The main function of the magnet is to generate a strong, stable and spatially uniform magnetic field. There are three different types of magnets used in MRI: a) Superconducting b) Permanent magnet and c) Resistive Electromagnets.

Permanent magnet has a limited magnetic strength, consume no electric power which is up to 1T and requires low or no maintenance. But higher magnetic field and are very stable. Magnets with high field strength are desired for clinical diagnosis and hence superconducting magnet is desired for clinical purposes.

Superconducting magnet can achieve high magnetic field but the maintenance cost of the magnet is higher due to its structure. It is made of superconducting wire (generally NbTi or NbSn alloys) with resistance approximately equal to zero when cooled to critical temperature: 0K (by immersing in liquid helium). The wire coil achieves superconducting state once it is below critical temperature and will remain in superconducting state without external power required to maintain current flow and field strength (27).

Resistive electromagnets are solenoids which generates magnetic field when current is passed through the solenoid. The magnetic field dies once the electric current is turned off. Due to natural resistance of wire, these magnets consume high amounts of electricity and it becomes expensive to operate above 0.3 T (27).

b) <u>RadioFrequency Coils</u>: The RF coils can function as transmitter of RF signal to the body or receiver of the RF signal from the body. Two separate transmission and reception coils are used for this purpose but a single coil can also achieve the purpose. The protons whose spins have same frequency as that of the transmission coil will receive the energy imparted and

get excited creating a condition of magnetic resonance. Transmission must be homogenous, therefore a large coil is preferred for transmission. Receiver coils detect the MR signal from the protons once the RF pulse is turned off. The receiver coils are generally placed close to the object as high sensitivity to object is important (14).

c) <u>Gradient Coils</u>: The gradient coil is an important hardware component of the MRI system. There are three set of gradient coils in each direction used to get spatial information. They play important role in slice selections and phase and frequency encoding. By varying the gradient frequencies we get precession frequency to be a function of spatial location

$$B(x,y,z) \rightarrow \omega(x,y,z) \hspace{5cm} (2.7)$$
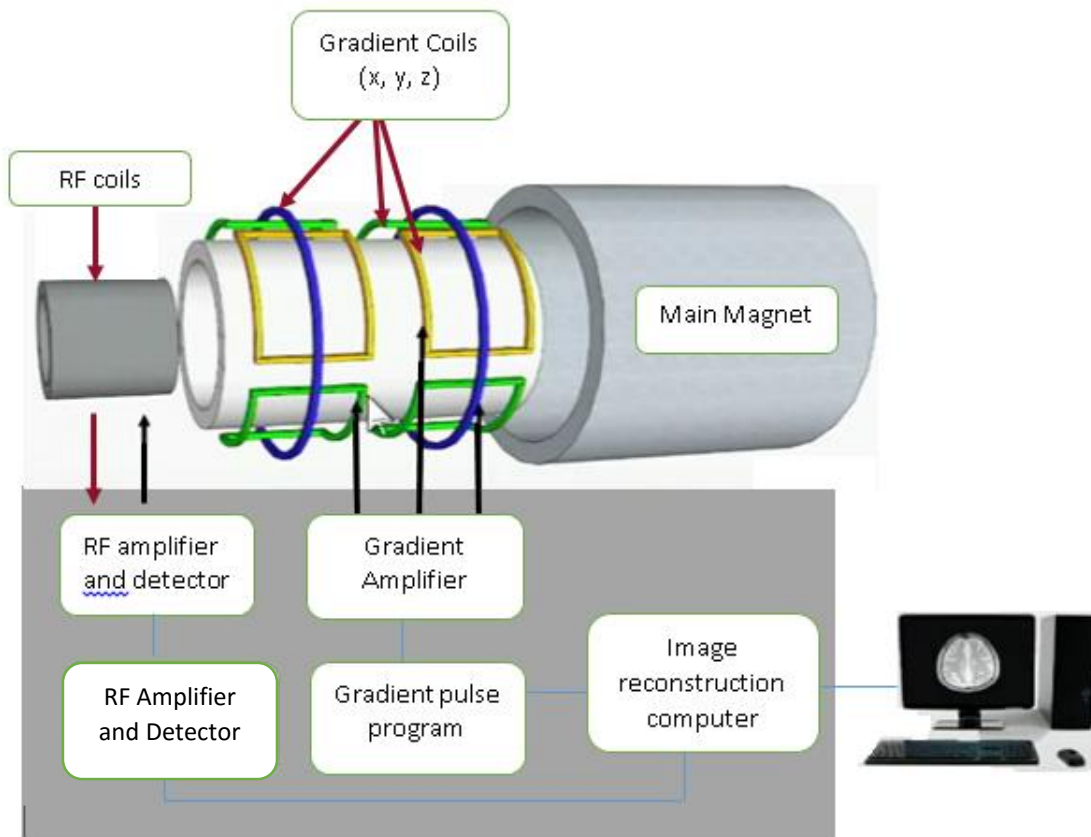
Figure 7: Schematic diagram of MRI hardware (adapted from14).

2.1.7 Pulse Sequences

A combination of RF and gradient pulses designed in time sequence are defined to form MR images from the acquired data. The schematic representation of these sequences represent the relative timing of the events taking place during an ongoing pulse sequence. Fourier transformation is applied to convert these signals from time domain to frequency domain. A pulse sequence typically consists of 4 lines at least, one being the RF transmitter and the remaining three representing the gradient coils. The two most important time parameters to consider in a pulse sequence are Repetition time (TR)

and Echo time (TE). The repetition time is the time between two consecutive 90 degree

RF pulses and echo time is the time between the RF pulse and echo.

The most common pulse sequence used in MRI is Spin echo sequence developed

by Edwin Hahn in 1950. A 90 degree excitation RF pulse is applied to tip the net

magnetization on transverse plane and a 180 degree RF pulse causes the spins to flip in

the transverse plane by reversing the spin phases: faster spins are where the slower ones

were and the slower ones are where the faster ones used to be. Now the spins precess

independently. This 180 degree pulse refocuses the spins and forms an echo.
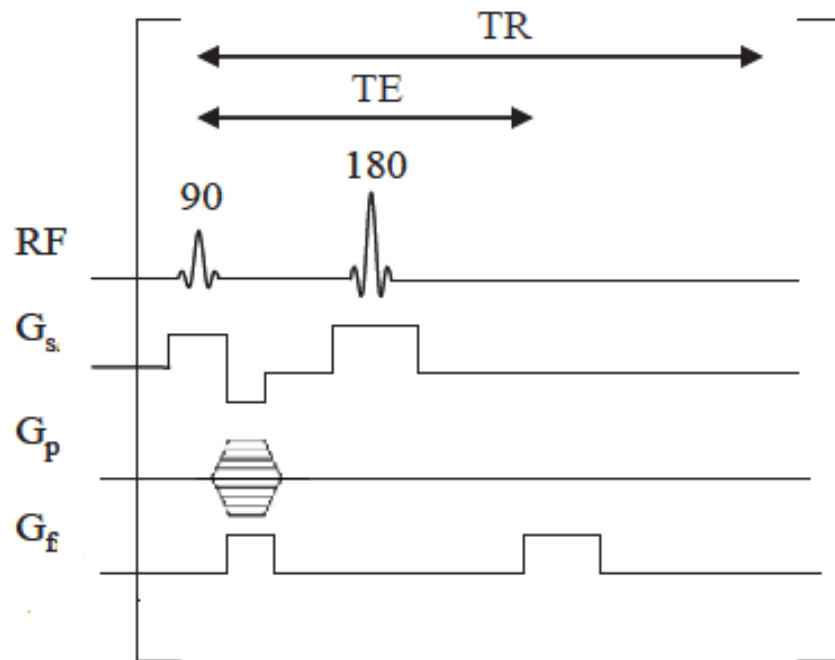
Figure 8: A simple time sequence diagram of spin echo sequence (adapted from 10).

Rapid Acquisition with Refocused images (RARE) uses image lines from multiple echoes i.e., it image acquisition is speeded up by acquiring more than one k-space line per repetition (28). This sequence begins with 90° RF pulse followed by refocusing 180° RF pulse like Spin echo sequence. It is followed by multiple 180° RF pulses to create many echoes also known as echo train. A different phase encoding gradient is applied to each echo to collect multiple k-space lines at once. Figure 9 shows a typical RARE sequence.
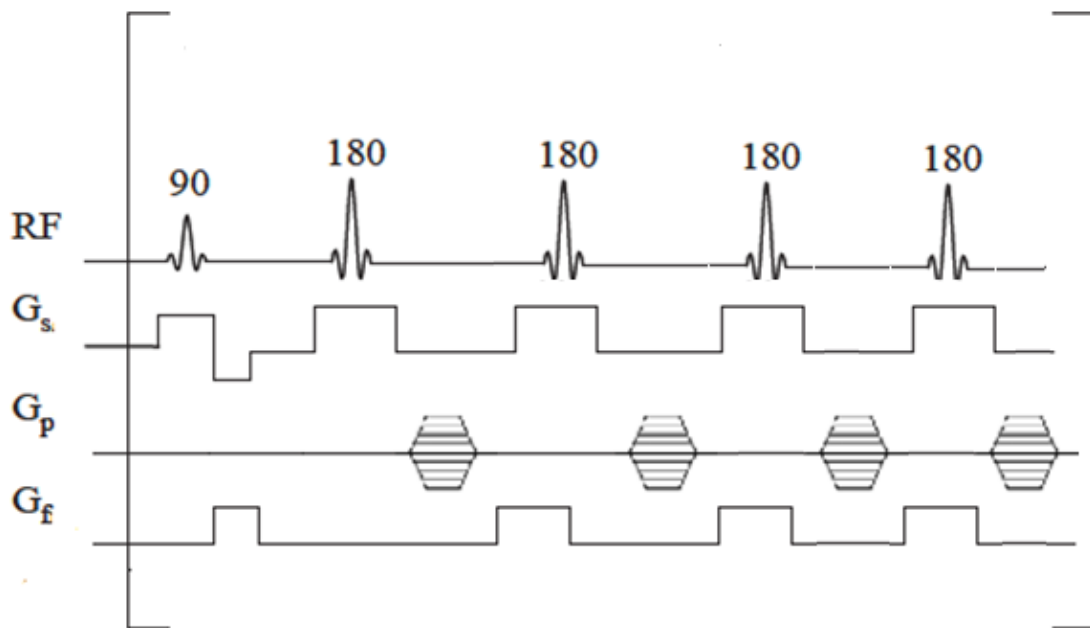
Figure 9. A typical RARE Sequence with four refocussing pulses (adapted from 27).

To measure T_2, a series of Spin Echo sequences can be applied by varying the TE and measuring the signal after each TE and it can be calculated from Eq 2.4. The multi slice multi echo pulse sequence (MSME) is commonly used sequence to measure T_2 and it uses Carr-Purcell-Meiboom-Gill (CPMG) pulse sequence with small variation (28). In CPMG, a 90° RF pulse is applied, followed by series of 180° RF and their corresponding echoes, known as echo train. In MSME the same sequence is repeated n number of times as shown in figure 8.
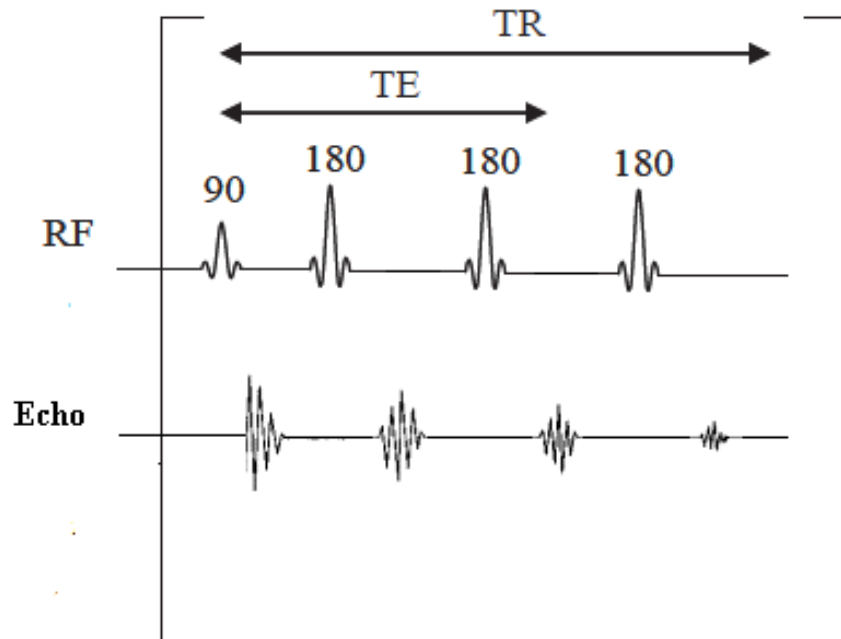
Figure 10: A simple timing sequence diagram illustrating multi slice multi echo time sequence.

2.2 <u>Diffusion MRI</u>

Diffusion can be defined as a mass transport process that results in mixing of molecules or particles in presence of concentration gradient without requiring bulk motion. It can be denoted by Fick's first law:

$$J = -D\nabla C \tag{2.8}$$

Where J is the net diffusion flux proportional to concentration gradient ∇C and D is the proportionality constant known as diffusion coefficient. The negative sign in the equation embodies the notion that the flow of molecules/particles is from higher concentration to lower concentration.

In the absence of concentration gradient, it is found that the particles still move and is known as molecular self-diffusion. It was first observed by Robert Brown and termed as 'random motion' or 'Brownian motion', later quantified by Einstein by using D from Fick's first law:

$$<x^2> = 2Dt \tag{2.9}$$

Where x is mean-squared displacement and t is diffusion time.

Diffusion can be measured using a pair of magnetic field gradients by varying the magnetic field over the region of interest. A pulsed gradient spin-echo is used to calculate the attenuated spin-echo signal caused by dephasing of the spins due to diffusion which can be achieved by application of two diffusion sensitizing gradient pulses. A 90 degree RF pulse is applied which is followed by diffusion sensitizing gradient pulse. Another

diffusion sensitizing gradient pulse is applied after 180 degree pulse is applied. If after the

application of diffusion sensitizing gradient pulses there is no change in position of the

particles due to diffusion, the net phase change becomes zero due to the two pulses

cancel out. However, if diffusion occurs, the net phase change does not become zero due

to incomplete cancellation resulting in phase dispersion and the overall signal gets

attenuated. The measured MR signal can be denoted as:

$$S = \ S_0 \, e^{-b(ADC)} \tag{2.10}$$

Where S and S_0 are the signal intensities obtained with and without diffusion gradient

respectively and b-value is a diffusion factor use to characterize the influence of gradients

on diffusion (10, 12).

 The b value for pulse gradient spin-echo can be denoted as:

$$b = \ \gamma^2 G^2 \delta^2 \left(\Delta - \frac{\delta}{3} \right) \tag{2.11}$$

where G is the gradient strength, Δ is separation and δ is duration. The term apparent

diffusion coefficient (ADC) is calculate by collecting two different set of data with two or

more b values. It reflects the diffusion in the direction of diffusion-weighting gradients

and the values are typically smaller in tissues compared to free water proton diffusion

values. The difference in b values generates the contrast in diffusion-weighting imaging

(DWI). Figure: shows the time sequence diagram for pulse gradient spin-echo sequence.
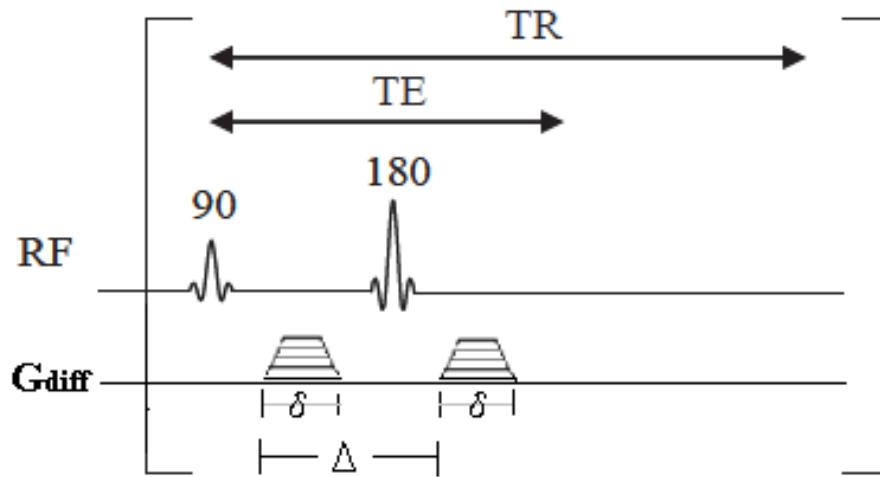
Figure 11: Time sequence diagram for pulse gradient spin-echo sequence (adapted from 12).

2.3 TISSUE ENGINEERING

Tissue engineering is a multidisciplinary field drawing experts from mechanical engineering, clinical medicine, materials science, genetics and related fields from both engineering and life sciences. Tissue engineering is a potential field that can overcome the shortage of donated organs by growing replacement tissues having potential to fully replace or regenerate the damaged organ. This developing field aims at regeneration of damaged tissues with the help of combining cells with porous scaffolds which provides structure and guides the growth of new tissue. Scaffolds provide appropriate environment and act as template for growth of tissues. They are seeded with cells and growth factors and are cultured in vitro to form tissues that can be implanted at the damaged site or can be implanted directly in to the injured site where in vivo tissue regeneration takes place (8).

2.3.1 <u>Principles of Tissue Engineering</u>

Cell is the basic functioning and structural unit of the body. They secrete their own support structure known as extracellular matrix which does more than just providing the framework, but also acts as relay station for various signaling molecules. It is necessary to understand how cells respond to the signals, organize in tissue and interact with the environment in order to mend damaged tissue and create new ones.

Stem cells used in tissue engineering can be autologous (stem cells from same person) or taken from other donor. They can be derived from different sources for example embryonic tissues, umbilical cord, and human bone marrow. The stem cells type typically used for bone or cartilage repair is human marrow derived mesenchymal stem cells (HMSCs).

These cells are seeded in a structure capable of supporting 3D tissue formation. This structure is typically known as scaffold. When the tissue is severely damaged the cells along with the tissue matrix called extracellular matrix (ECM) gets damaged and scaffolds acts as a substitute for ECM. The main functions of scaffolds are to provide 3D structure for tissue formation, allowing cell attachment and proliferation, enabling diffusion of cell nutrients and creating an environment that enables cell growth and neotissue formation. The two types of biomaterials used for scaffold formation are: natural and synthetic. Mechanical properties, biocompatibility and bioadsorbability defines their basis of selection for being used for tissue formation. Some common biomaterials used are:

chitosan, collagen, fibrin, elastin, etc. and some common polymers used are: Poly (Glycolic Acid) [PGA], Poly (L-Lactic Acid) [PLLA], Poly (ethylene glycol) [PEG], etc. (6).

Growth factors are regulatory biomolecules (proteins) that bind to the receptors on cell surface and activates cellular differentiation/proliferation. Cytokines are also protein that help in cellular function, communication and embryogenesis. Different types of growth factors are used depending on the tissue site where regeneration will takes place. Some commonly used growth factors are: platelet derived growth factors (PGFs), insulin like growth factors (IGFs), fibroblast growth factors (FGFs), bone morphogenic proteins (BMPs) etc.

Cells   +   scaffold   +   Bioactive factors   =   Engineered tissue construct
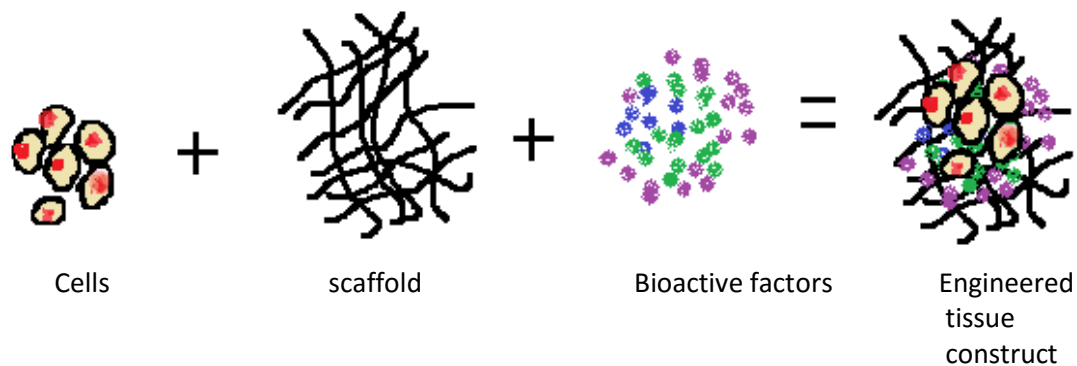
Figure 12: Basic procedure followed in tissue engineering. Shows the basic building blocks: cells, scaffold and bioactive factors.

Human bone is made up of collagen fibers and inorganic bone minerals. Bone contains 10% - 20% of water and 50% - 60% of the dry mass of bone is bone minerals. Rest of bone is collagen fibers (main fibrous protein) and it also consists of small amount inorganic salts and proteins. Cartilage is also a collagen based tissue and has large polysaccharide molecules that entangles the collagen fibers together in the gel formed by

these molecules. Cartilage is softer than bone and articular cartilage is found on the bearing surface of the movable joints (23).

The wear of articular cartilage occurs due to various reasons like sports injury, trauma, osteoarthritis etc. The damage to cartilage exposes the underlying subchondral bone which further damages the underlying bone. The tissue engineered cartilage has properties similar to the components of the native cartilage but with higher amount of stem cells and chondrocytes. It also has higher amount of proteoglycans than collagen. The current treatment options for damaged cartilage are: treatment using bone marrow stimulation, osteochondral autograft transfer system and autologous chondrocyte implantation (21, 22). These treatments are not yet adequate enough for restoring the cartilage function for a long term. The tissue engineered scaffolds have potential to repair and regenerate the damaged bone and cartilage but they fail in translation from pre-clinical to post clinical implantation due to lack of appropriate noninvasive monitoring and assessment tools. Currently, the techniques used to assess the engineered tissue are destructive processes like histological and biochemical analysis which can be only applied at the end of tissue culture. The studies explained in further sections are expected to provide the required noninvasive tools that has potential to monitor the tissue growth at any required stage.

3. MR ASSESSMENT OF LEUCINE ZIPPER BASED SCAFFOLD

The LZ based scaffolds utilized in this study used LZ hydrogels as scaffold material. These hydrogels are self-assembling hydrogels with tunable properties. The self-assembling nature results in dense interconnected fibrillar microstructures. The scaffolds are strong enough to support cell structure and their mechanical strength can be regulated by adjusting the LZ hydrogel concentration in scaffold. The LZ hydrogels are stable and can be stored at room temperature for several months once they are lyophilized. They are porous in nature with pore size ranging from 20μm - 100 μm and the pore size can be controlled by adjusting the composition of the hydrogel (3).

3.1 Materials and Methods

3.1.1 Scaffold Preparation

LZ Control scaffold were prepared using self-assembling LZ hydrogels. LZ hydrogels (3). LZ hydrogels were prepared by mixing specific ratios of the LZ-Control protein with LZ-RGDS at specific concentrations and dissolving in 100 mM phosphate buffer. Formation of LZ self-assembling hydrogel took place within three hours of incubation at 37°C. For further physical crosslinking and sterilization, the hydrogel was then lyophilized and baked at 121°C for 12 hrs. Hydrogels were stored in sterile containers at room temperature.

The LZ control scaffold was modified in two sets of LZ scaffold used in this experiment, high ECM and low ECM integrated. The low ECM integrated scaffolds were prepared by culturing 25,000 HMSCs within the control LZ scaffolds and the high ECM

were prepared by culturing 50,000 HMSCs within the control LZ scaffolds. Both the scaffolds were cultured in regular HMSC culture media for 2 weeks. The scaffolds were then decellularized as per published protocols (4, 5) and lyophilized.

3.1.2 <u>Scanning Electron Microscopy</u>

The scanning electron microscopy was performed on LZ hydrogels by quenching them in liquid nitrogen and then placing them in pre-cooled turbo freeze-drying chamber. The samples were dried in series of steps ranging from -160°C to room temperature in the increments of 20°C per hour at ultra-low pressure of 1 x 10^{-3} mmHg. The samples, once dried, were fractured to expose the inner structure and were mounted onto SEM grid. 10nm osmium tetroxide coat was applied on samples and the imaging was performed using a Field Emission Hitachi S-4800-II SEM operating at 5 keV. The microstructure of the lyophilized fractures surface of Control, Low ECM and High ECM integrated scaffolds in phosphate buffer can be observed in the SEM images, figure 12.
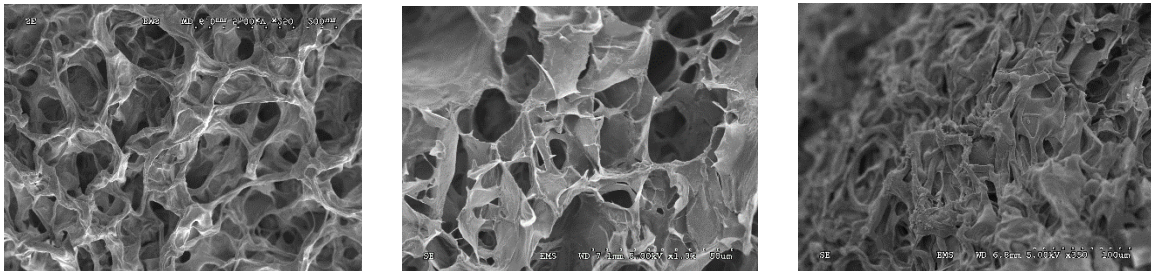

Figure 13 : SEM Images of LZ scaffolds: Control, Low and High ECM.

3.1.3 <u>Proton MRI Experiments</u>

All the samples were imaged using Bruker 11.7T (500MHz) vertical bore magnet using a 5mm Proton RF coil and the imaging software Paravison 4.0. The osteogenic samples were hydrated using the 1X Phosphate Saline Buffer (PBS) for 20 minutes before putting them into 5mm NMR tubes. The NMR tubes were prepared by filling it with 1% Agarose gel till the required height and the samples were put on top of agarose gel. Fluorinert oil was used to fill the remaining volume of the tube. The T_1 parametric maps for all the three samples (Control ECM, High ECM and Low ECM) were obtained using RAREVTR (RARE with variable TR) pulse sequence and the experimental parameters were: TE = 12ms, TR = 1200ms, 1767ms, 2561ms, 3000ms, 10000ms, FOV = 8mm x 8mm, matrix size = 128 x 128, slice thickness = 1mm and. The T_2 relaxation time measurements were made using MSME (multi slice multi echo) pulse sequence with the experimental parameters: TE = 7.2ms, TR = 2000ms, FOV = 8mm x 8m, matrix sixe = 128 x 128 and slice thickness = 1mm. The apparent diffusion coefficient (ADC) was obtained through the diffusion weighted spin echo sequence with the experimental parameters: TE = 25ms, TR = 2000ms, b values (mm^2/s) = 100, 250, 500, 750, 1000, FOV = 8mm x 8mm, matrix sixe = 128 x 128 and slice thickness = 1mm. The T1, T2 and ADC maps were obtained though custom written MATLAB program. The system was calibrated using agarose gel. The data obtained is listed in the table II.

Figure 14: LZ scaffolds in the 5mm NMR tubes.

3.2 Results

Data analysis was done using a custom written MATLAB program (for T1, T2 and ADC). The ROI were defined on the basis of threshold that covered the entire sample. The tabulated results in Table III shows the average of data from 5 slices and the threshold intensity was maintained same for each slice analyzed in a particular scan.

From Table II we can see significant decrease in the values for T_1 and T_2 as we go from low to high ECM integrated LZ scaffolds. There was no statistically significant difference (performed student's t-test) in the values of ADC were seen and the values of diffusion were similar to diffusion coefficient of free water proton.

26

LZ scaffolds (n = 5) and Agarose Gel	Proton relaxation times in Fluorinert oil		
	T_1 (s)	T_2 (ms)	ADC x 10^{-3}(mm^2/s)
Control	2.1$\pm$ 0.3	59.33 $\pm$ 1.4	2.1 $\pm$ 0.1
Low ECM	2.06$\pm$ 0.4	53.7 $\pm$ 2.5	2.0 $\pm$ 0.1
High ECM	1.7 $\pm$ 0.6	40.78 $\pm$ 1.2	2.0 $\pm$ 0.08
Agarose Gel	1.5 $\pm$ 0.7	43.3 $\pm$ 0.6	1.98 $\pm$ 0.07

Table II: T_1, T_2 and ADC values of the LZ control, Low ECM and High ECM scaffolds.
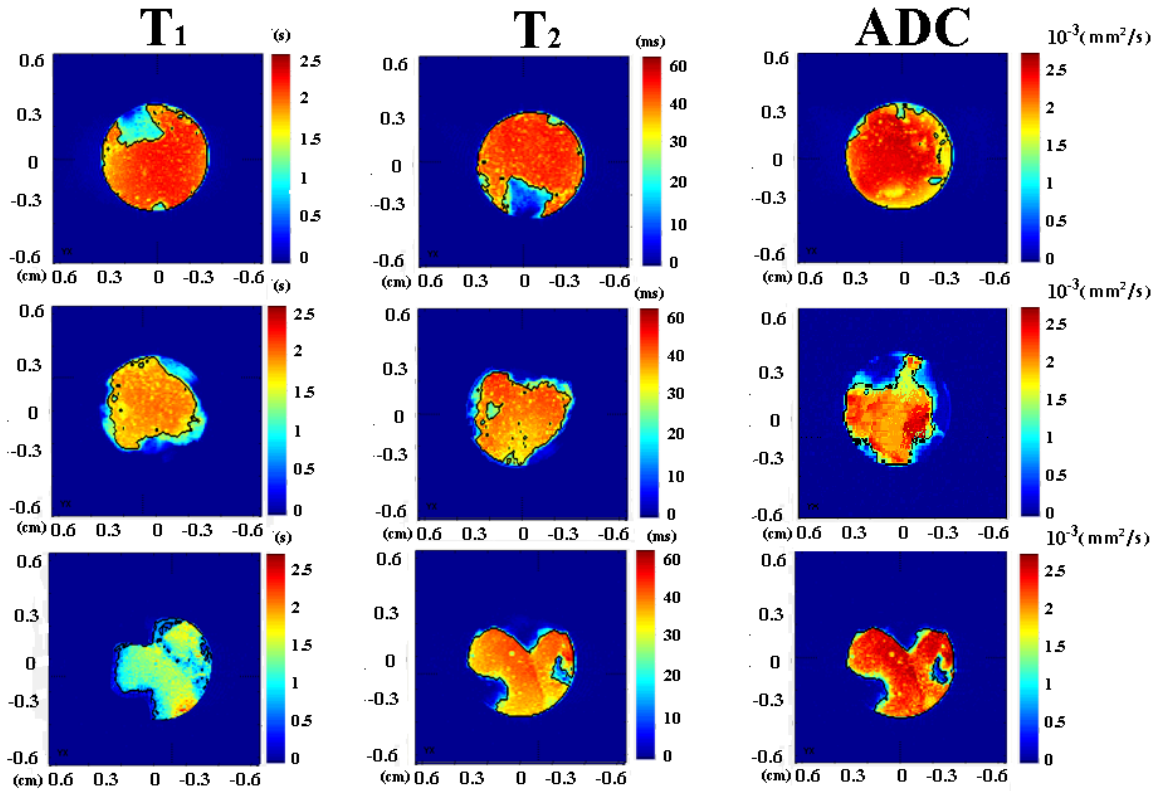

Figure 15: T_1, T_2, and ADC maps for LZ scaffolds: Control, Low ECM and High ECM.
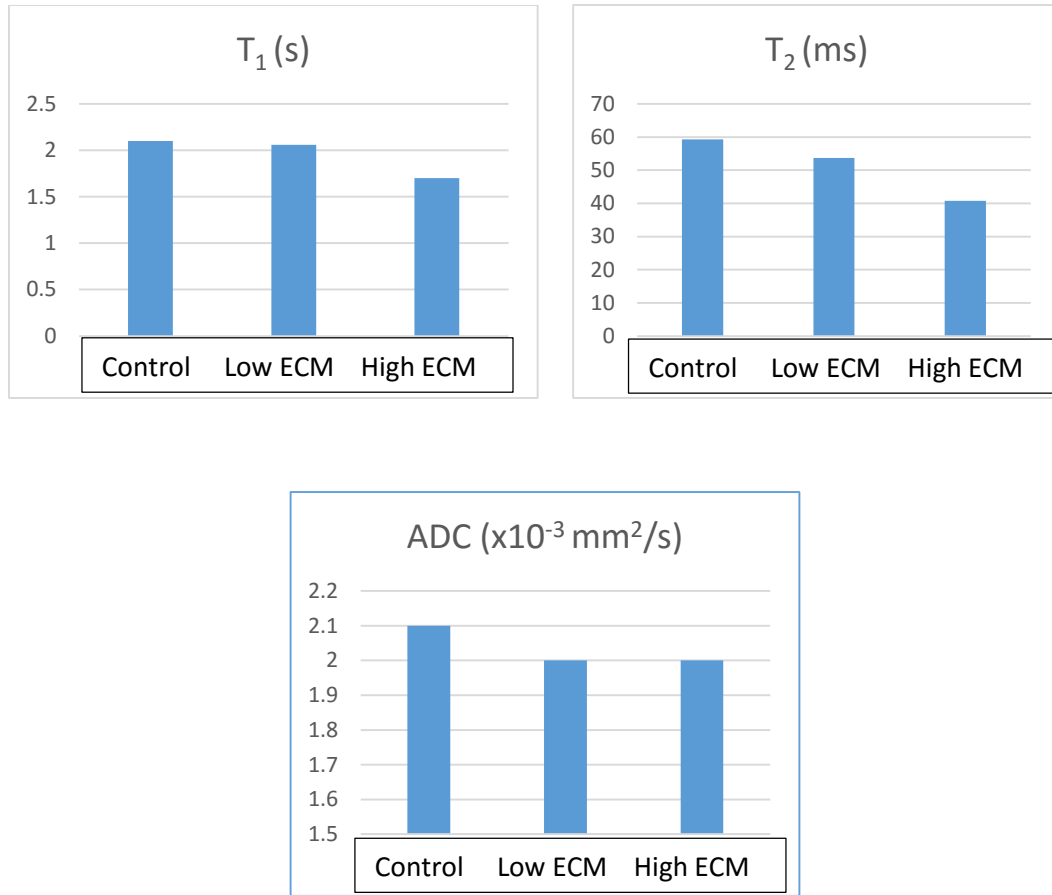
Figure 16: Histogram showing MRI measurements of LZ Scaffolds: control, Low ECM and High ECM

3.3 Discussion

Tissue stiffness cannot be directly measured through these experiments but it indicates the changes in tissue stiffness. According to the Bloembergen-Purcell-Pound (BPP) theory of water relaxation, the ratio T_2/T_1 is an indication of the water environment as shown. The smaller ratio for high ECM constructs is a sign of complex or more solid osteogenic ECM generated in the high ECM tissue engineered construct when compared to low ECM and control tissue engineered constructs. Therefore, high ECM bone tissue constructs are stiffer than low ECM bone tissue constructs (25, 16).

3.4 <u>Conclusion</u>

This study shows that MRI is sensitive to the structural and composition changes in the tissue engineered bone. Through MRI it is evident that these scaffolds were successful in production of osteogenic ECM as also confirmed by the biochemical analysis. MRI has the potential to monitor and assess the small structural and growth changes in the tissue noninvasively.

4. <u>MRI ASSESSMENT OF CHONDROGENIC SCAFFOLDS</u>

This study utilizes the commercially available Zimmer clinical grade collagen tape and modifies it under two sets of conditions to be used as chondrogenic scaffolds. The goal of this study is to evaluate the properties of the modified scaffolds and through this study we will be able to determine which scaffold is the better construct for clinical uses.

4.1 <u>Materials, Methods and Results</u>

4.1.1 <u>Scaffold Preparation</u>

The control scaffold used in this study was Zimmer clinical grade collagen tape. The chondrogenic ECM scaffold were prepared under two set of conditions: a) Normoxia: normal oxygen conditions and b) Hypoxia: low oxygen conditions. Chondrogenic ECM scaffold - Normoxia was created by culturing 10 million human bone marrow derived mesenchymal stem cells (HMSCs) in the control collagen scaffold for two weeks under the influence of chondrogenic differentiation media. The cells were then decellularized as per published protocols (5) to remove the cells and cellular material and leave behind the incorporated ECM within the collagen framework. The chondrogenic ECM scaffold – Hypoxia was prepared by culturing 10 million HMSCs under hypoxic conditions (2% oxygen) controlled by elevating the partial pressure of Nitrogen and under the influence of chondrogenic differentiation media. The scaffolds were then decellularized as per published protocols (5).

4.1.2 Immunohistochemical Analysis

Immunohistochemical analysis were performed using Vecta Stain peroxidase kit (Vector labs) as per manufacturer's protocols and developed using DAB kit (Vector Labs). The analysis showed the presence of various ECM components present in bone matrix. It revealed the presence of non-collagenous proteins (NCPs) known for playing significant role in differentiation of mesenchymal cells. Further the mechanical testing performed on control, normoxia and hypoxia scaffolds shows hypoxia is a better construct with better ultimate tensile strength but lower toughness (5).
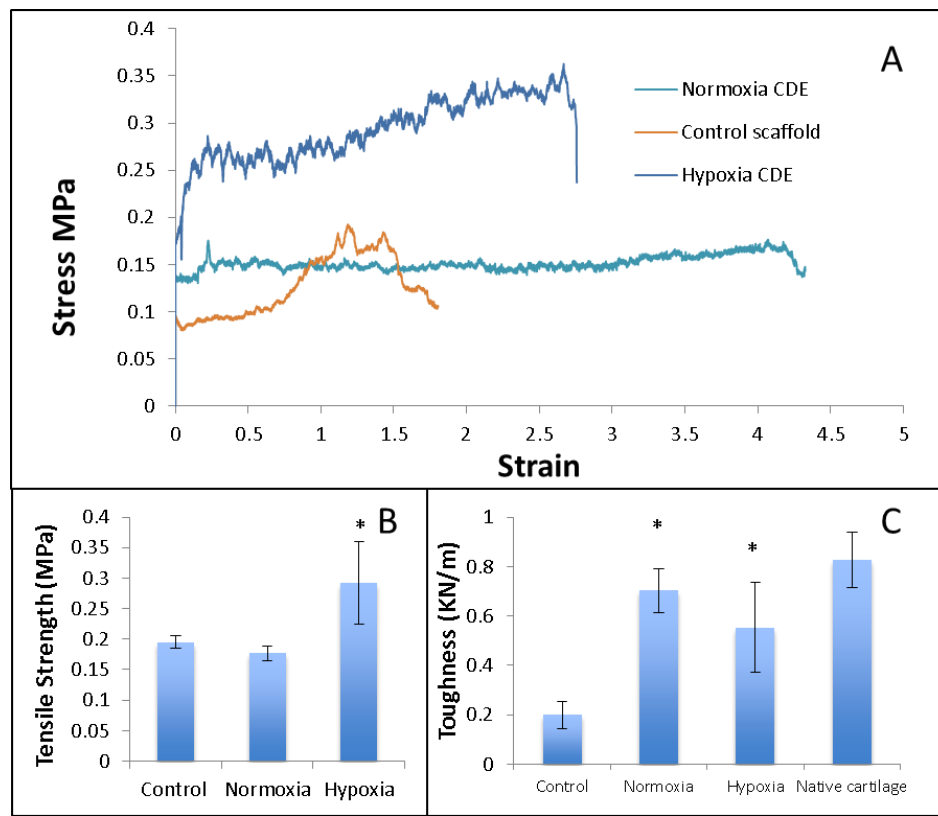

Figure 17: Mechanical testing performed on Control, normoxia and hypoxia chondrogenic scaffolds.

4.1.3 Proton MRI Experiments

The MRI measurements were performed on Bruker Avance 11.7T (50MHZ) vertical bore magnet using a 5mm Proton RF coil. The chondrogenic scaffolds were hydrated using the chondrogenic media overnight before putting them into 5mm NMR tubes. The NMR tubes were prepared by filling it with 1% Agarose gel till the required height and the samples were put on top of agarose gel. Fluorinert oil was used to fill the remaining volume of the tube. The T_1 parametric maps for all the three samples (commercially available Control scaffold, modified version of the commercially available scaffold: Normoxia scaffold created under normal oxygen condition, Hypoxia scaffold created under low oxygen condition) were obtained using RAREVTR (RARE with variable TR) pulse sequence and the experimental parameters were: TE = 11.5ms, TR = 1200ms, 1767ms, 2561ms, 3000ms, 10000ms, FOV = 8mm x 8mm, matrix size = 128 x 128, slice thickness = 1mm and. The T_2 relaxation time measurements were made using MSME (multi slice multi echo) pulse sequence with the experimental parameters: TE = 7.2ms, TR = 2000ms, FOV = 8mm x 8mm, matrix sixe = 128 x 128 and slice thickness = 1mm. The apparent diffusion coefficient (ADC) was obtained through the diffusion weighted spin echo sequence with the experimental parameters: TE = 17.8ms, TR = 2000ms, b values (mm^2/s) = 100, 250, 500, 750, 1000, FOV = 8mm x 8mm, matrix sixe = 128 x 128 and slice thickness = 1mm. The T_1, T_2 and ADC maps were obtained though custom written MATLAB program. The system was calibrated using agarose gel. The data obtained is listed in the table II.

Figure 18: The 11.7 Tesla Bruker Imaging System located at Research Resources system at University of Illinois at Chicago.

4.2 Results

Data analysis was done using a custom written MATLAB program (for T_1, T_2 and ADC). The ROI were defined on the basis of threshold that covered the entire sample. The tabulated results in Table III shows the average of data from 5 slices and the threshold intensity was maintained same for each slice analyzed in a particular scan.

From table III we can see significant decrease in the values for T_1 and T_2 as we go from normoxia to hypoxia scaffolds. There was no statistically significant difference (performed student's t-test) in the values of ADC between different constructs and the values of diffusion were similar to diffusion coefficient of free water proton.

Chondrogenic scaffolds (n = 5)	Proton relaxation times in Fluorinert oil		
	T_1 (s)	T_2 (ms)	ADC x 10^{-3}(mm^2/s)
Control	2.6 ± 0.36	36.8 ± 1.5	1.97 ± 0.01
Normoxia	2.3 ± 0.35	30.7 ± 0.9	1.90 ± 0.03
Hypoxia	1.8 ± 0.5	30.08 ± 1.0	1.94 ± 0.04

Table III: MRI measurements of chondrogenic collagen scaffold: Control, Normoxia and Hypoxia.

4.3 Discussion

Tissue stiffness cannot be directly measured through these experiments but the results indicates the changes in tissue stiffness. As discussed in previous study, according to the Bloembergen-Purcell-Pound (BPP) theory of water relaxation, the ratio T_2/T_1 is an indication of the water environment as shown. The smaller ratio for hypoxic constructs is a sign of complex or more solid chondrogenic ECM generated when compared to control

and normoxic constructs. Therefore, hypoxia tissue engineered cartilage constructs are stiffer normoxia tissue engineered constructs (25, 26).
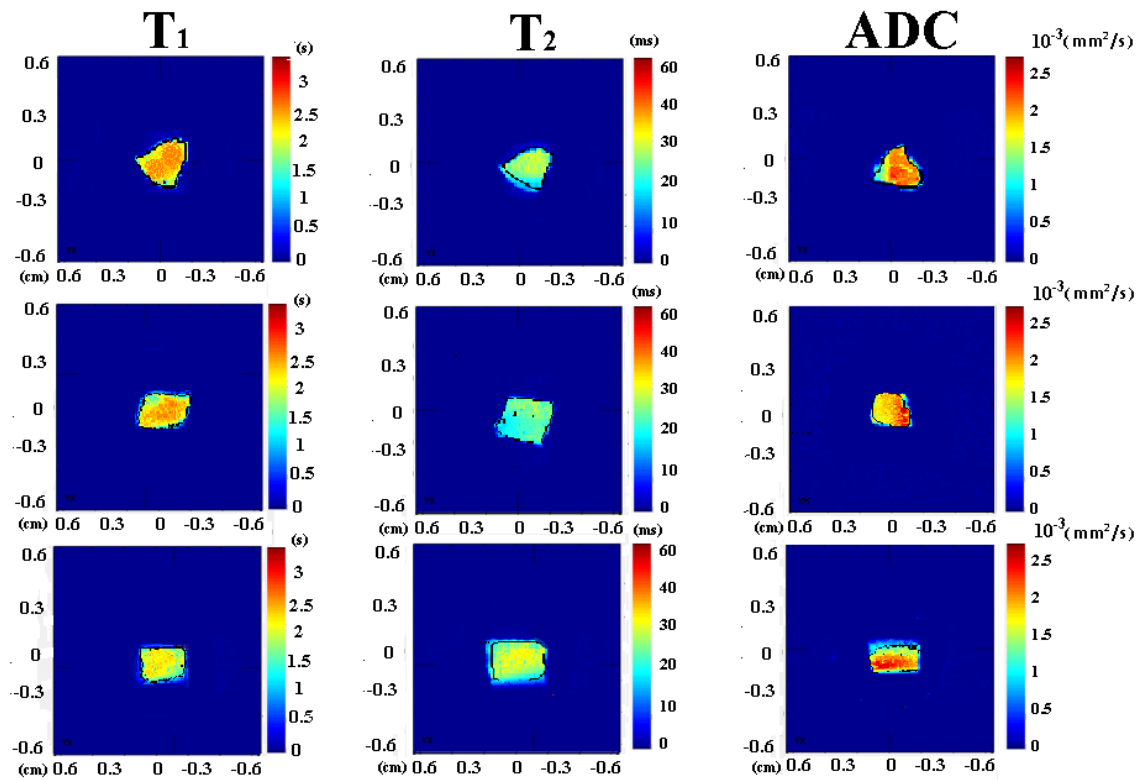

Figure 19: T_1, T_2, and ADC maps for Chondrogenic scaffolds: Control, Normoxia and Hypoxia
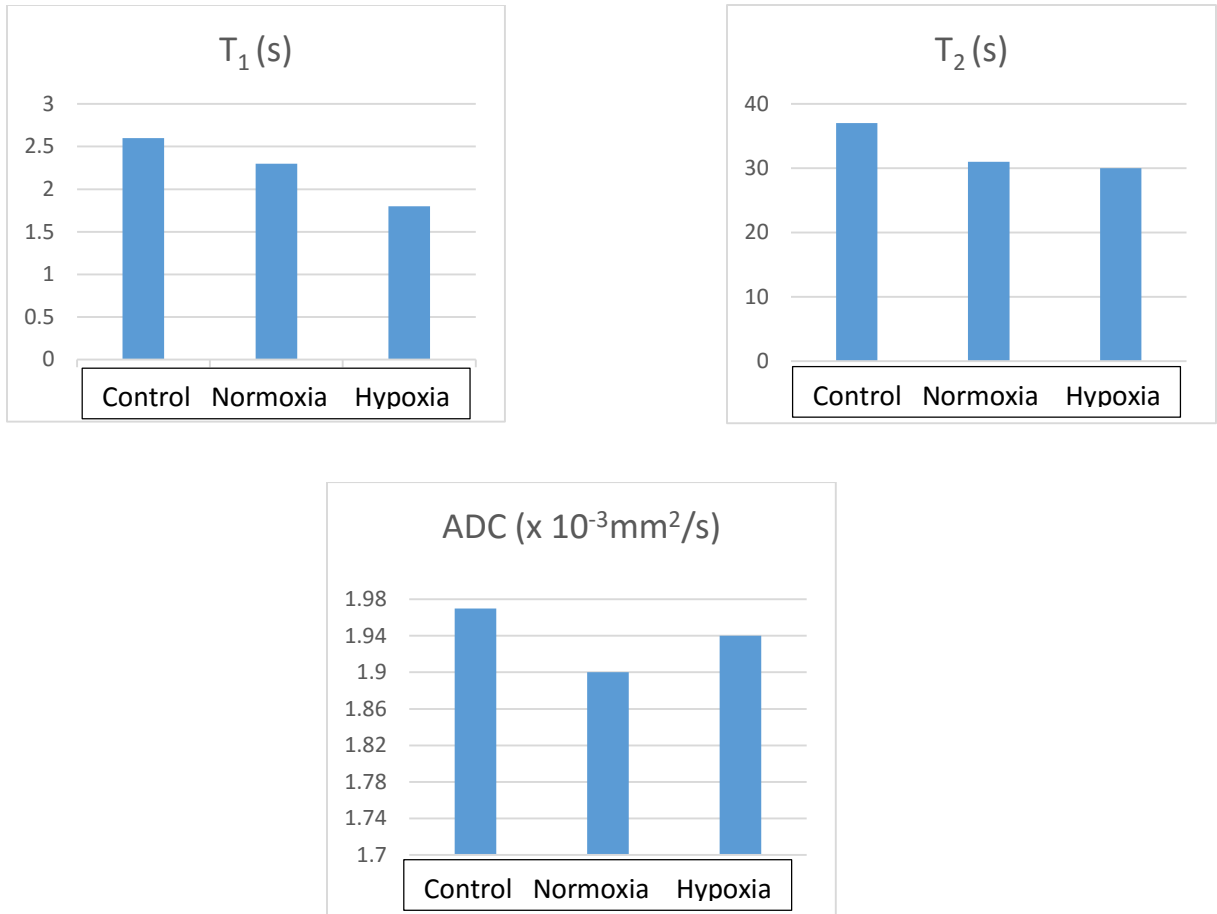
Figure 20. Histogram showing the MRI measurement results for Chondrogenic scaffolds.

4.4 <u>Conclusions</u>

This study shows that decrease in the values of T_1 and T_2 of normoxic and hypoxic constructs compared to the control scaffold shows that the scaffolds were successful in producing chondrogenic ECM. MRI is successful in detecting the changes in the tissue noninvasively which is also detected by biochemical analysis.

5. CONCLUSIONS AND FUTURE WORK

This study concludes that MRI is sensitive in detecting small structural changes in tissue engineered bone and cartilage. The decrease in the proton relaxation times shows the increased stiffness in the tissues as we go from normoxia to hypoxia for engineered cartilage and from low and high ECM integrated biomimetic scaffolds for engineered bone. This increase in the level of stiffness can be attributed to the growth of extracellular matrix in hypoxic and high ECM integrated scaffolds which also shows that these scaffolds are also capable of producing ECM without the need of adding growth factors. The statistically insignificant change in the values of apparent diffusion coefficient shows the normal diffusion of nutrients and oxygen taking place in the scaffolds. The studies show that it is possible to conduct longitudinal assessment on the same tissue construct without destroying the tissue. The parameters evaluated by MRI would enable screening of the engineered bone and cartilage. This would eliminate the tedious and destructive biochemical approaches that are being currently used. Further work is underway to apply $T_{1\rho}$ and Sodium MRI experiments on both sets of scaffolds.

6. REFERENCES

1. Huihui Xu, Shadi F. Othman, Richard L. Magin, "Monitoring Tissue Engineering Using Magnetic Resonance Imaging", Journal of Bioscience and Bioengineering 106(6): 515-527, ISSN 1389-1723: 2008.

2. Clair, B.L., A.R. Johnson, and T. Howard. "Cartilage repair: current and emerging options in treatment". Foot Ankle Spec, 2(4): 179-88, 2009.

3. Huang, C. C., S. Ravindran, Z. Yin and A. George, "3-D self-assembling leucine zipper hydrogel with tunable properties for tissue engineering." Biomaterials 35(20): 5316-5326: 2014.

4. Ravindran, S., Q. Gao, M. Kotecha, R. L. Magin, S. Karol, A. Bedran-Russo and A. George. "Biomimetic extracellular matrix-incorporated scaffold induces osteogenic gene expression in human marrow stromal cells." Tissue Eng Part A 18(3-4): 295-309: 2012.

5. Ravindran, S., C.-C. Huang, P. Gajendrareddy and R. Narayanan, Biomimetically Enhanced Demineralized Bone Matrix for Bone Regenerative Applications. Frontiers in Physiology 6: 2015.

6. Ravindran, S., M. Kotecha, C. C. Huang, A. Ye, P. Pothirajan, Z. Yin, R. Magin and A. George, Biological and MRI characterization of biomimetic ECM scaffolds for cartilage tissue regeneration. Biomaterials 71: 58-70: 2015.

7. R. H. Hashemi, W. G. Bradley, and C. J. Lisanti, MRI: the basics. Lippincott Williams & Wilkins, 2012.

8. Fergal J. O'Brien, "Biomaterials & scaffolds for tissue engineering, Materials Today", 14 (3): 88-95, ISSN 1369-7021: 2011.

9. Yin Z. MR Relaxation, Diffusion, and Stiffness Characterization of Engineered Cartilage Tissue [dissertation]. ; 2014.

10. N. B. Smith and A. Webb, "Introduction to Medical Imaging Physics Engineering and Clinical Applications", 2010th ed. Cambridge University Press, pp. 157–219.

11. M. Kotecha, D. Klatt, and R.L. Magin (2013). "Monitoring cartilage tissue engineering using magnetic resonance spectroscopy, imaging, and elastography", Tissue Eng. Part B, Reviews, 19, (6): 470-484.

12. Yin Z. "Magnetic resonance characterization of tissue engineered cartilage via changes in relaxation times, diffusion coefficient, and shear modulus." Critical reviews in biomedical engineering; 42(2):137-91, 2014.

13. R. H. Hashemi, W. G. Bradley, and C. J. Lisanti, "MRI: the basics". Lippincott Williams & Wilkins, 2012.

14. Sung-Hong Park, "MRI Fundamentals" [Online]. Available: https://class.coursera.org/mrifundamentals-001.

15. M. Kotecha, D. Klatt, and R.L. Magin. "Monitoring cartilage tissue engineering using magnetic resonance spectroscopy, imaging, and elastography", Tissue Eng. Part B, Reviews, 19, (6): 470-484, 2013.

16. P. J. Basser and E. Özarslan, "Introduction to Diffusion MR," Diffusion MRI: From Quantitative Measurement to In vivo Neuroanatomy: Second Edition, pp. 3–9, 2013.

17. "Basic Physics of Nuclear Medicine/MRI & Nuclear Medicine." [Online]. Available: http://en.wikibooks.org/wiki/Basic_Physics_of_Nuclear_Medicine/MRI_&_Nuclear_ Medicine.

18. M. Brown, R. Semelka, and T. K. Nishino, "MRI: Basic Principles and Applications, 3rd edition," *Medical Physics*, vol. 31. p. 170, 2004.

19. J. P. Hornak, "The Basics of MRI." [Online]. Available: http://www.cis.rit.edu/htbooks/mri/inside.htm.

20. Lanza R. P., Langer, Robert S., Vacanti J. "Principles of tissue engineering 4th Edition". Academic Press; 2013

21. Kotecha, M., S. Ravindran, T. M. Schmid, A. Vaidyanathan, A. George and R. L. Magin. "Application of sodium triple-quantum coherence NMR spectroscopy for the study of growth dynamics in cartilage tissue engineering." NMR Biomed 26(6): 709-717, 2013.

22. Marolt, D., M. Knezevic and G. V. Novakovic. "Bone tissue engineering with human stem cells." Stem Cell Res Ther 1(2): 10, 2010.

23. "Structure of bone and Implant Materials" [Online]. Available at http://www.doitpoms.ac.uk/tlplib/bones/structure.php

24. Pearle, A. D., R. F. Warren and S. A. Rodeo. "Basic science of articular cartilage and osteoarthritis." Clin Sports Med 24(1): 1-12, 2005.

25. Pothirajan P, Ravindran S, George A, Magin RL, and Kotecha M*, "Magnetic resonance spectroscopy and imaging can differentiate between engineered bone and engineered cartilage, IEEE-EMBC proceedings", 3929 – 3932, 2014.

26. N. Bloembergen, E.M. Purcell, and R.V. Pound: "Relaxation Effects in Nuclear Magnetic Resonance Absorption", Physical Review, 73, (7), pp. 679-712, 1948.

27. Kenneth W. Fishbein, Joseph C. McGowan, and Richard G. Spencer, "Hardware for Magnetic Resonance Imaging", 2005.

28. J. Ross, "Integrated Magnetic Resonance Centre for Doctoral Training", 2012.

HEMANTI CHAVADA

Education

- Masters of Science in Bioengineering   Aug 2014 – May 2016

  University of Illinois at Chicago

  Thesis Title: "In vitro Magnetic Resonance Assessment of Tissue Engineered bone

  and cartilage."

- Bachelors of Technology in Computer Science   July 2009 – June 2013

  Gujarat Technological University

Research Experience

- Department of Bioengineering, University of Illinois at Chicago, IL   Jan 2015 – May 2016

  Magnetic Resonance Quantification of tissue engineered bone and Cartilage

Conference Abstract

- Hemanti Chavada, Chun-Cheih Huang, Sriram Ravindran, Richard Magin, Mrignayani Kotecha; "In vitro MR Assessment of Tissue Engineered Bone and Cartilage" submitted for presentation at 8th Midwest Regional Conference of the AIChE at Chicago, IL, Mar 3-4, 2014.